Alongshore winds force warm Atlantic Water toward Helheim Glacier in southeast Greenland

Tasha Snow[1], Weifeng Gordon Zhang[2], Erika Schreiber[3], Waleed Abdalati[3], and Ted Scambos[4]

[1]Colorado School of Mines
[2]Woods Hole Oceanographic Institution
[3]University of Colorado Boulder
[4]US National Snow and Ice Data Center

November 22, 2022

Abstract

Enhanced transport of warm subsurface Atlantic Waters (AW) into Greenland fjords has driven glacier mass loss, but the mechanisms transporting AW to the fjords remain poorly characterized. Here, we identify a wind-driver for AW inflow toward Sermilik Fjord abutting Helheim Glacier, one of Greenland's largest glaciers. Often associated with the passing of cyclones and subsequent sea surface lowering, a weakening or reversal of northeasterly alongshore winds stimulates coastal ocean upwelling that, through interactions with Sermilik's bathymetric trough on the continental shelf, leads to enhanced AW upwelling and inflow along the trough. These intrusions produce ocean warming at deep moorings near Sermilik Fjord mouth (0.31±0.18°C) and within the fjord (250m: 0.30±0.19°C; 350m: 0.17±0.09°C) that is not diminished by subsequent coastal downwelling. Similar wind-driven processes at other bathymetric trough regions around Greenland may play a substantial role in ocean heat transport towards much of the Greenland Ice Sheet.

Alongshore winds force warm Atlantic Water toward Helheim Glacier in southeast Greenland

T. Snow[1,2,3], W. Zhang[4], E. Schreiber[5], W. Abdalati[2,3], T. Scambos[2]

[1]Colorado School of Mines, Department of Geophysics, Golden, CO, USA
[2]Cooperative Institute for Research in Environmental Sciences, University of Colorado, Boulder, CO, USA
[3]University of Colorado Boulder, Geography Department, Boulder, CO, USA
[4]Applied Ocean Physics and Engineering Department, Woods Hole Oceanographic Institution, Woods Hole, MA, USA
[5]UNAVCO, 6350 Nautilus Drive, Boulder, CO, 80301, USA

Key Points:

- Alongshore wind-driven coastal upwelling near Sermilik Fjord drives intrusions of Atlantic Water onto the continental shelf
- Intrusions often lead to warmer subsurface water in the inner shelf and fjord
- Less transport within the East Greenland Coastal Current makes fjords more susceptible to Atlantic Water intrusions

Corresponding author: Tasha Snow, `tasha.snow@colorado.edu`

Abstract

Enhanced transport of warm subsurface Atlantic Waters (AW) into Greenland fjords has driven glacier mass loss, but the mechanisms transporting AW to the fjords remain poorly characterized. Here, we identify a wind-driver for AW inflow toward Sermilik Fjord abutting Helheim Glacier, one of Greenland's largest glaciers. Often associated with the passing of cyclones and subsequent sea surface lowering, a weakening or reversal of northeasterly alongshore winds stimulates coastal ocean upwelling that, through interactions with Sermilik's bathymetric trough on the continental shelf, leads to enhanced AW upwelling and inflow along the trough. These intrusions produce ocean warming at deep moorings near Sermilik Fjord mouth (0.31±0.18°C) and within the fjord (250m: 0.30±0.19°C; 350m: 0.17±0.09°C) that is not diminished by subsequent coastal downwelling. Similar wind-driven processes at other bathymetric trough regions around Greenland may play a substantial role in ocean heat transport towards much of the Greenland Ice Sheet.

Plain Language Summary

Higher transport of the warm subtropical Atlantic Waters into Greenland fjords has driven glacier mass loss, but the mechanisms transporting the subtropical waters to glacier fronts remain poorly characterized. In this work, we identify a wind mechanism for transporting subtropical water towards Helheim Glacier, one of Greenland's largest glaciers. Often associated with the passing of cyclones, alongshore wind events stimulate ocean circulation that brings subtropical waters from offshore onto the continental shelf along a submarine trough that leads to Helheim. Our measurements show that when these events produce ocean warming near-shore, they may help to transport more heat to Helheim Glacier front where it can cause enhanced ice melting. A higher number of wind events in a season has the potential to impact glacier calving, thinning, and retreat. These events may also occur along other bathymetric troughs leading toward Greenland glaciers and, therefore, may be important for predicting future Greenland Ice Sheet ice loss.

1 Introduction

The Greenland Ice Sheet is now the leading contributor to global sea level rise each year and approximately half of this mass loss results from outlet glacier dynamics (speedup, thinning, and retreat) at its periphery (Enderlin et al., 2014; Mouginot et al., 2019; IMBIE Team, 2019; Smith et al., 2020). Helheim Glacier - one of the largest glacier in Greenland - has experienced multiple dynamic ice loss events over the past two decades, as have other neighboring glaciers in southeastern Greenland (Howat et al., 2008; Murray et al., 2010). These regionally synchronous events were likely triggered by enhanced submarine melting by the ocean; acceleration, thinning, and retreat at Helheim corresponded to warming waters and enhanced ocean heat transport into Sermilik Fjord, the fjord that abuts Helheim (Holland et al., 2008; Mouginot et al., 2015; Millan et al., 2018). It is unclear, however, what mechanisms modulate that ocean heat transport from the broader ocean into the fjords through time and, thus, what may have triggered the past glacier retreat events.

Transport of relatively warm (2.0-5.2°C) Atlantic-origin subsurface waters (AW; found from 150-250 m to the seafloor) delivers much of the ocean heat to Helheim Glacier front and can vary substantially as a result of highly variable ocean circulation (Straneo et al., 2010; Jackson et al., 2014). Within Sermilik Fjord, relatively cold (<4°C) and fresh Polar-origin water (PW) resides at the surface above AW in a two-layer circulation structure (Straneo et al., 2010; Sutherland et al., 2014). The dominant mode for variability within these layers is an oscillatory "intermediary" circulation caused by wind-driven coastal geostrophic currents and changing offshore water mass properties (Svendsen & Thompson, 1978; Straneo et al., 2010; Jackson et al., 2014; Fraser et al., 2018). Under this highly dynamic circulation scheme, alongshore northeasterly (prevailing) winds drive Ekman transport shore-ward at the surface and create a compensating flow offshore at depth (Håvik & Våge, 2018), resulting in coastal ocean downwelling (Figure 1b). During such downwelling, the sea surface height can rise ∼15 cm (Jackson et al., 2014; Cowton et al., 2016), isopycnals heave downwards (Straneo et al., 2010; Jackson et al., 2014), and the PW layer thickens. Opposing southwesterly winds drive the opposite set of changes (Figure 1c). Ocean pressure gradients between the coastal waters and the fjord, created by coastal downwelling or upwelling, drive rapid current reversals within intermediate layers of Sermilik Fjord on synoptic timescales of 4-10 days (Jackson et al., 2014). These intermediary currents can be strong enough to flush the upper 300 m of the fjord within ∼4 days if persistent and therefore have the potential to drive large water and heat exchanges with the shelf (Straneo et al., 2010; Sciascia et al., 2014). The wind-driven circulation sometimes leads to changed water properties within the fjord, but can also result in oscillations with no net change in water properties (Jackson et al., 2018). It is unclear what distinguishes these two.

Outside the fjord, a complex circulation system allows AW to intrude onto the continental shelf (∼300-400 m deep) along a bathymetric trough (∼15 km wide, ∼400-900 m deep) that leads to Sermilik Fjord and Helheim (Figure 1b,c; Sutherland et al., 2013; Harden et al., 2014; Snow et al., 2021). The East Greenland Coastal Current (EGCC) flows at the surface along the coast carrying PW equatorward (Sutherland & Pickart, 2008), and AW spreads onto the shelf beneath it. Offshore, the Irminger Current (IC) carries AW southward throughout the upper 500 m (Rudels et al., 2002; Johannessen et al., 2011; Våge et al., 2011; Andresen et al., 2012), which can be diverted onto the shelf (Sutherland et al., 2013; Harden et al., 2014; Snow et al., 2021). Aside from general in-

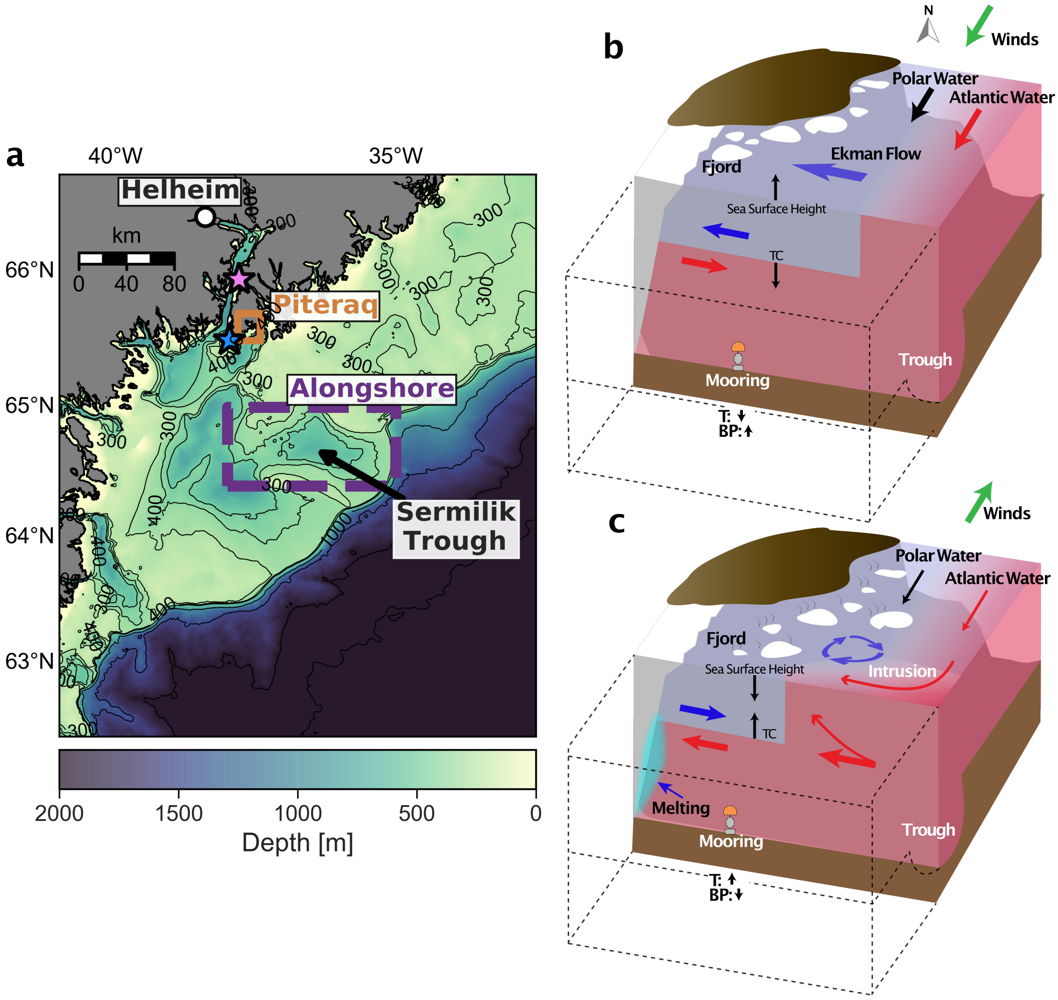

Figure 1. The Sermilik Trough study region and wind-driven ocean circulation along the trough. (a) Bathymetry for the continental shelf near Sermilik Fjord and Trough. Sampling locations for the ERA-5 reanalysis alongshore winds (purple dashed) and piteraqs (orange) are shown (see Methods). Stars indicated the shelf (blue) and mid-fjord (pink) mooring locations. Bathymetry is from BedMachine v3 with the thin black lines representing contours at 300, 400, 500 m, and every 500 m thereafter (Morlighem et al., 2017). (b,c) Also shown are schematics of the ocean circulation along Sermilik Trough during winds favoring (b) downwelling and (c) upwelling. Arrows indicate Polar Water (blue) and Atlantic Water (red) flow direction. Clockwise-rotating purple arrows indicate the vorticity created by coastal-trapped waves, which stimulates Atlantic Water intrusion along the trough. White and brown features indicate ice and land, respectively. We use the following abbreviations: TC (thermocline), BP (bottom pressure), and T (temperature).

flow at depth, full-depth AW inflow occurs on synoptic timescales along the trough or as seasonally-varying inflow across portions of the shelf. AW intrudes further onto the shelf in the fall and is associated with a narrower EGCC banked up against the coast

(Harden et al., 2014; Snow et al., 2021). Intrusions of AW may be linked with EGCC transport variability (Murray et al., 2010), cyclonic eddies (Bruce, 1995; Sutherland & Pickart, 2008; Sutherland et al., 2013), tidal variability, or fluctuations in alongshore winds (Hampson, 2020). However, little work has been done in the shelf region to link the broader ocean and fjord during these events, so the drivers of the intrusions and linkages to water property changes inshore remain unclear.

Here, we use MODIS optical imagery and sea surface temperatures (SST) from the continental shelf region near Sermilik Fjord to characterize intrusions of AW, their drivers, and how they impact shelf and fjord subsurface water temperatures. Unlike previous work on AW variability within Sermilik Fjord and near the fjord mouth, we produce a comprehensive shelf-wide study of AW intrusion and its variability from 2010-2013 when we have coincident moored ocean observations. We investigate mechanisms driving these intrusions using ECMWF (European Center Medium-Range Weather Forecasts) reanalysis data, sea surface height, and SST-derived EGCC variability. We show that coastal upwelling, often caused by upwelling-favorable winds generated by the passing of a cyclone and subsequent sea surface height lowering, drive these intrusions. We use moored subsurface ocean temperature records from the continental shelf and fjord to determine the impacts that the intrusions have on subsurface ocean temperatures that may eventually reach Helheim Glacier. Our findings suggest that an interplay between EGCC transport and wind variability plays a large role in ocean heat transport into Sermilik Fjord, and potentially other fjords in southeastern Greenland.

2 Background

A timeseries of MODerate Resolution Imaging Spectroradiometer (MODIS) optical images from February 27th to March 4th, 2013 reveals the evolution of a rapid AW intrusion cross-cutting from the slope to inner continental shelf near Sermilik Fjord (Figure 2a). The intrusion bisected the EGCC, which was, at the time, choked with seasonal sea ice, making the intrusion observable with optical imagery. Just before the intrusion on February 27th, sea ice hugged the coast flowing to the south under prevailing northeasterly winds that had persisted for most of the preceding seventeen days according to ECMWF reanalysis data. Clouds from two cyclonic systems passing by late on February 27th and 28th precluded visibility of the surface, but winds shifted early on February 28th briefly and again March 1st to blow at ∼10 m/s from a northwesterly direction

(250°to 350°) off the ice sheet, where they remained for the next two days. In imagery from the afternoon of March 1st, the intrusion had snaked across >40 km of the EGCC within the last two days bringing AW from the offshore IC almost to the mouth of Sermilik Fjord along the northeastern flank of the Sermilik Trough. Observed through MODIS Band 31 (thermal infrared)-derived brightness temperatures, portions of the AW intrusion were ∼4°C warmer than surrounding EGCC and fjord waters (Figure S1c). March 2nd imagery (Figure 2a) shows the remnants of the intrusion being encroached upon by sea ice within the EGCC and surface outflow from Sermilik Fjord, both moving to the south with the current. By the 4th when winds returned to their prevailing northerly direction, sea ice had been pushed southward covering the Sermilik Trough region, and the cross-shelf intrusion was no longer visible. This phenomenon has not been previously studied, and its influence has not been accounted for in large-scale models. Intrusions of this kind may rapidly advect AW and heat into Sermilik Fjord and toward Helheim Glacier and may therefore serve as an important factor in glacier dynamics (Figure 1c).

Data and Methods

AW intrusions are observable throughout the MODIS record near Sermilik Fjord, and they appear to vary widely in size and extent. To characterize these intrusions and determine their frequency and variability in time, we initially identify AW intrusion events along the Sermilik Trough using MODIS optical imagery from NASA WorldView (see Table S1, Figure 2a). The intrusions were selected from a larger set in the observable record to be clearly illustrative of the processes involved, and are identified by both the ice-free water cross-cutting the EGCC, as well as the surface outflow from fjords (i.e. open water streaming to the south) that follows. We make these observations from 2010 to 2013 when simultaneous moored temperature records exist for the region, and only for January through June when sea ice cover along the EGCC makes the intrusions readily identifiable in the visible spectrum. Optical identification of the intrusions restricts our observations to AW intrusions that have surface expressions; therefore, intrusions that do not fully penetrate to the surface are unobserved. Further, cloud cover frequently obscures observations of the ocean surface. Thus, our observations include only a fraction of the total intrusion events during the study period, but the available data sets support a clear characterization of the processes.

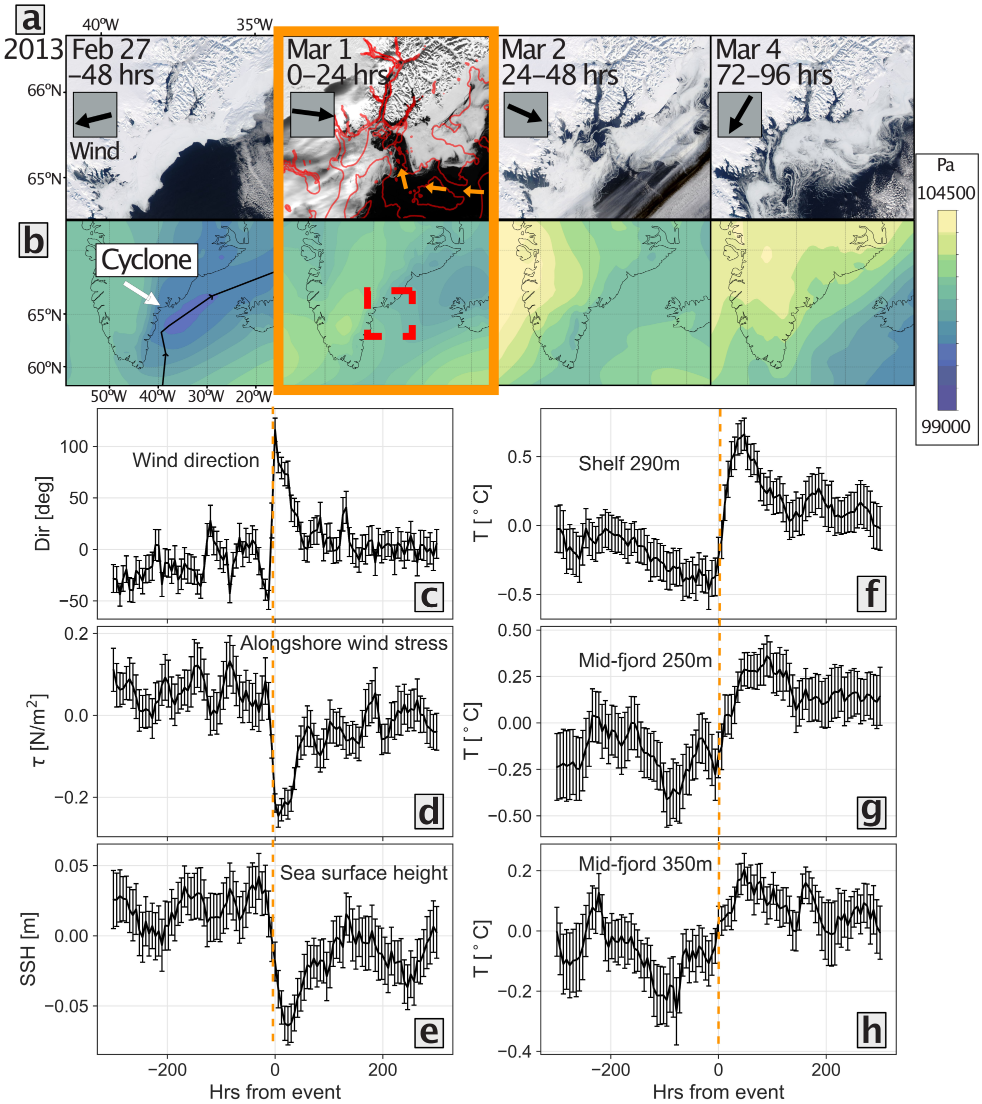

Figure 2. Evolution of Atlantic Water (AW) intrusions near Sermilik Fjord. (a) MODIS optical imagery of an AW intrusion from Feb 27th to Mar 4th, 2013. Hours refers to hours before (negative) or since (positive) the shifting of alongshore wind stress and initiation of the intrusion (orange). Wind direction and relative speed are depicted by the arrows within gray boxes. The red contours indicate the 250 m and 500 m isobaths, which show the location of Sermilik Trough. Orange arrows indicate the right-hand side of the trough and the path of AW shown in Figure S1. (b) Mean sea level pressure for each time step. A cyclone is shown with the black lines indicating the cyclone track. The red box indicates the location of the images in panel (a). (c-h) Composites of atmospheric and ocean parameters during fifty-three (53) identified AW intrusion events (see Results): (c) ERA-5 wind direction, (f) alongshore wind stress (positive means northeasterly), (e) sea surface height (SSH), and mooring temperatures from (f) the continental shelf near Sermilik Fjord mouth (290 m) and mid-fjord at (g) 250 m and (h) 350 m depth. The onset of negative alongshore wind forcing is shown by the orange lines, and hours are the same as in (a).

Synoptic-scale ocean circulation in the Sermilik Trough region may have ties to weather conditions, such as wind patterns. Previous work in Sermilik Fjord (Straneo et al., 2010; Jackson et al., 2014, 2018) and along the southeastern coast of Greenland (Sutherland & Pickart, 2008; Oltmanns et al., 2014; Le Bras et al., 2018) has shown strong correlations between ocean circulation patterns and various wind drivers, including cyclones and piteraqs (hurricane intensity downslope winds in the off-shore direction), supporting the notion that winds may influence these intrusions. Here we investigate the influence of atmospheric variability on the intrusions using atmospheric reanalysis data from the ECMWF ERA-5 operational reanalysis data set (Copernicus Climate Change Service (2017) ERA-5). From ERA-5, we use the 6-hourly 2-m wind field, instantaneous turbulent surface stresses, and mean sea level pressure fields to determine the atmospheric variability before and after the intrusions. From the ERA-5 U and V wind speeds and stress, we calculate the northeasterly alongshore wind at the shelf break (Figure 1a; see Supplemental Information). A positive alongshore northeasterly wind component specifies downwelling-favorable winds along the coast; a negative southwesterly wind specifies upwelling. To investigate the influence of cyclones, cyclone frequency and tracks are derived from ERA-5 records using an advanced cyclone detection and tracking algorithm as described in Crawford and Serreze (2016) and Crawford et al. (2020). Piteraqs (or Downslope Wind Events) were identified following Oltmanns et al. (2014) (Figure 1a; see Supplementary Information).

We investigate the extent to which intrusions affect ocean properties nearshore and within Sermilik Fjord by examining ocean temperature changes and sea surface height (SSH) during the intrusions. We use mooring temperature data from the continental shelf within the trough leading to Sermilik Fjord and within the fjord (Figure 1a), which were both deployed multiple times between August 24, 2009 - August 18, 2013 (see Supplementary Information; Jackson et al., 2014; Harden et al., 2014; Jackson & Straneo, 2016). The shelf mooring was deployed $\sim$290 m depth near the mouth of Sermilik Fjord. We also use SSH records from Harden et al. (2014), which were calculated from bottom pressure measurements at the same shelf mooring. The mooring within the fjord was located mid-fjord - 32 km from the shelf mooring and $\sim$70 km from the Helheim Glacier front - at $\sim$250, $\sim$350, $\sim$400, and $\sim$550 m depth. These moorings provide a time varying record, averaged to 6-hourly time steps, of subsurface AW that is known to flow onto the continental shelf and into Sermilik Fjord (Straneo et al., 2011; Jackson & Straneo, 2016) and would likely detect ocean property changes associated with the variability of AW intrusions at depth.

Prominence of the EGCC may also affect intrusion of AW onto the continental shelf (Murray et al., 2010). To investigate this possibility, we obtain the width of the EGCC during the intrusions using MODIS SST-derived observations of PW extent based on Snow et al. (2021) with small refinements (see Supplementary Information).

Results

We visually identified fifty-three (53) intrusion events during winter and spring (January to June) between 2010 and 2013 (see Table S1, Figure S2). All intrusions are marked by ice-free waters – warmer than the surrounding EGCC and fjord surfaces – cutting through the sea ice covered EGCC along Sermilik Trough. We interpret these as an inflow of AW at the surface. In several of the more distinct intrusions, cross-shelf velocities of the intrusion flow were 0.13-0.19 m/s based on the distance that the intrusions crossed within a 24-hour period (e.g., 10.9-16.2 km for May 20, 2010 and March 26, 2010, respectively). Within 24-48 hours after the intrusion becomes visible, outflow at the surface is indicated by outward spreading of sea ice and cool PW away from the coast except along the trough, and by relatively ice-free waters flowing out of Sermilik Fjord to the south within the EGCC.

Shifts in alongshore wind velocity and SSH preceded, and appear to drive, the AW intrusion events (Figure S2). Intrusions most frequently occurred after the passing of a low pressure (LP) system (87% of selected intrusions) and less frequently with only a high pressure (HP) system nearby (11%). Winds during most of the intrusion events took two forms within the 24 hours preceding the intrusions: i) winds that shifted from the prevailing northeasterly direction to a westerly direction, and ii) winds that weakened following strong northeasterly wind stresses (typically >15 m/s; Figure S2); the latter occurred less frequently (13 of the events). Intrusions also often coincided with a drop in SSH. These wind and SSH patterns are consistent with a transition from a wind-driven coastal downwelling regime – building sea surface height, depressing isopycnals, and causing inshore surface flow and offshore bottom flow along Greenland's southeastern coast – to a relaxation of that build-up or, more commonly, to upwelling conditions, which leads to the opposite oceanic response (Håvik & Våge, 2018). Fjord outflow visible at the surface during the intrusions (Figure 2a) - which are consistent with fjord intermediary flow driven by coastal upwelling - support this notion (Straneo et al., 2010; Jackson et al., 2014). Only two intrusions occurred under persistent, weaker downwelling-favorable winds, though, they both coincided with cyclones passing over the Irminger Sea and one was associated with an ∼30 cm drop in SSH. Other influences such as tides and cyclonic eddies propagating along the continental slope (Bruce, 1995; Magaldi et al., 2011; Brearley et al., 2012; Sutherland & Pickart, 2008) may moderate intrusions, but we rule them out as primary forcing mechanisms because of the frequencies mismatch between those phenomena (sub-daily to 1-2 days) and the less frequent AW intrusions (>2 days). We also rule out piteraqs, which rarely coincide with AW intrusions (11%; see Table S1) and do so only when upwelling-favorable wind conditions simultaneously occurred offshore.

The reanalysis and moored ocean records confirm the close linkages between the intrusions, alongshore wind stress, SSH, and inshore ocean warming. Alongshore wind stress and SSH records have a strong positive correlation ($r=0.36$, $p<0.001$) and both had significant negative correlations with the mooring records from the shelf at 290 m, mid-fjord at 250 m and mid-fjord at 350 m depth ($r=-0.19$ to -0.24 with wind stress, $r=\sim-0.32$ with SSH, $p<0.001$; see Supplementary Information). These negative correlations are consistent with a downwelling-to-upwelling switch in coastal conditions. It is difficult to distinguish between temperature changes associated with the heaving of isopycnals vertically in the water column and lateral advection of warm water into the fjord without closer examination of the changes across intrusion events.

To examine the effect of the shift from downwelling to upwelling favorable winds, we create composites of the atmospheric and ocean variability during the intrusions to identify linkages (Figure 2c). To build the composite, we normalized each of the parameters by their mean over the period spanning 300 hours before and after the times of downwelling-to-upwelling wind shift that occurs within the 24 hours preceding the imagery-indicated intrusion events. We then average across all identified intrusions events.

Both the satellite and mooring observations show a shift to warmer ocean temperatures on the shelf and in the fjord that persists for at least eight days after the intrusions (Figure 2c). MODIS brightness temperatures revealed surface water temperatures (Figure S1) within the intrusions could be ∼4°C warmer than those in the EGCC and fjord, similar to AW temperatures within the IC. Further, when we use mean temperature differences from the 4 days before and 4 days after the events ($\Delta T_{4,-4}$) as an indication of temperature change, the intrusions corresponded with significant warming at the shelf mooring (0.71±0.13°C) and mid-fjord moorings at 250 m (0.44±0.13°C), 350 m (0.24±0.08°C), and 400 m (0.08±0.05°C), though not at 550 m (0.01±0.03°C). The warming trend held for $\Delta T_{4:8,-4:8}$ (difference between temperatures averaged over 4-8 days before and 4-8 days after the wind events) at all moorings between 250 and 400 m (shelf: 0.31±0.18°C; mid-fjord 250m: 0.30±0.19°C; mid-fjord 350m: 0.17±0.09°C; mid-fjord 400m: 0.09±0.07°C). These indicate that the intrusions led to sustained warming in the upper AW layer (250-400 m deep; Figure S1) through laterally transporting warm AW to the shelf and fjord, rather than merely producing the vertical heaving of isopycnals (Jackson et al., 2014).

Our finding that the AW intrusions produce significant warming inshore at the surface and at depth indicates enhanced upwelling and shoreward transport of AW along Sermilik Trough. Subsurface warming at the fjord mouth and mid-fjord are consistent with our satellite-based findings that the intrusions drive warm surface water inshore toward Sermilik Fjord. The subsurface warming within the fjord show that this water is also transported into the fjord at depths of 250 and 400 m and potentially the entire AW layer. Further, the co-occurrence of shoreward flow in the Sermilik Trough with the shift in alongshore winds and SSH align with the finding of Zhang and Lentz (2017) that upwelling-favorable winds (Hampson, 2020) or a relaxation of strong downwelling-favorable winds can drive strong onshore cross-shelf flow in a shelf valley (see below).

While the majority of all intrusions (79% for the +4-day window, 55% for the 4 to 8-day window) resulted in warming on the shelf, exceptions exist. On an event-by-event basis, sustained ocean warming occurred frequently (92% on the shelf and approximately two-thirds in the fjord) when the EGCC was narrow (<61±14 km), and less frequently (42% on the shelf and ∼35% in the fjord) when the EGCC was wider. These findings indicate that the width of the EGCC and therefore transport (see Supplemental Information), moderate AW intrusion inshore, which is consistent with previous research finding that EGCC width increases the dilution of AW as it crosses the continental shelf (Snow et al., 2021). Other factors that may impact the recorded warming signals inshore include variability in source water temperature or a rapid temperature fluctuation obscuring our temperature metric. For instance, a coastal downwelling occurring 4-8 days after an intrusion would be considered by our analysis as a cooling event.

Discussion

Shoreward flow of AW replenishes heat at depth within the interior of the continental shelf and the fjords along SE Greenland, and herein we have described an alongshore wind mechanism that actively pumps AW inshore along the trough leading to Sermilik Fjord. We show that upwelling-favorable wind events drive AW upwelling and inflow toward Sermilik Fjord within the trough (Figure 2, S1). These conditions are most often driven by cyclones (LP systems) and, less frequently, anti-cyclones (HP). 79% of the identified intrusions lead to subsurface warming at moorings near the fjord mouth (290 m) and >50% of the intrusions lead to warming mid-fjord (250 m and 400 m). These increase the amount of heat flowing toward Helheim Glacier.

We provide a holistic description of the AW intrusion events that links wind-driven fjord and continental shelf processes (Figure 1). During downwelling-favorable winds (Figure 1b), the EGCC flows faster (Le Bras et al., 2018), isopycnals depress, and the sea surface raises $O(15\text{cm})$ toward the coastline on the shelf (Jackson et al., 2014; Harden et al., 2014; Håvik & Våge, 2018). Water along the coast experiences a negative density anomaly and positive bottom pressure anomaly (indicating a positive sea-surface height anomaly) (Harden et al., 2014) that propagates up-fjord (Jackson et al., 2014). Within the fjord, the PW layer thickens as water flows in at the surface, isopycnals heave downwards, the subsurface warm layer thins as AW flows out of the fjord, and the sea surface rises (Straneo et al., 2010; Jackson et al., 2014). When this prevailing wind mode transitions to upwelling-favorable winds (Figure 1c), the fjord and shelf experience an opposite effect, lifting warm dense AW onto the shelf, driving a shore-ward flow of the AW, and causing PW surface outflow from the fjord and coast (Jackson et al., 2014; Håvik & Våge, 2018). This upwelling response can eject freshwater and sea ice off the continental shelf on the surface (Oltmanns et al., 2014; Håvik & Våge, 2018).

We propose that the Sermilik Trough bathymetry facilitates the onshore intrusion of AW. It results from asymmetric responses of the trough circulation to the ambient along-shelf flows of opposite directions when the Rossby number, Ro=U/(fL), of the tough flow is $\mathcal{O}(1)$ (Lentz et al., 2014; Zhang & Lentz, 2017; Hampson, 2020). Here, U is a scale of the along-shelf flow, f the Coriolis Parameter, and L a length scale of the trough. The observed onshore intrusion of the AW along the northeastern flank of the Sermilik Trough is consistent with upwelling flow on upstream canyon slopes (Allen & Hickey, 2010; She

& Klinck, 2000; Zhang & Lentz, 2017). During upwelling-favorable winds or sudden reduction in downwelling-favorable winds, water along the northeastern flank of the trough upwells and flows shore-ward throughout the entire water column, lifting dense AW from the continental slope toward Sermilik Fjord (Figure 1). This onshore flow at the trough is either a part of a steady standing coastal-trapped wave that is excited at the trough and then arrested by the northeastward shelf flow, or a transient consequence of the excessive onshore pressure gradient force associated with the greater water depth in the trough (Allen & Hickey, 2010). During downwelling-favorable winds, enhancement of the offshore flow in a canyon/trough is minimum (Allen & Madron, 2009; Lentz et al., 2014), consistent with topographically generated coastal-trapped waves propagating freely downstream (to the southwest in this case) away from the trough. Therefore, downwelling- and upwelling-favorable winds do not drive equivalent opposing flows along the trough and oscillatory along-shelf winds can generate localized net onshore inflow in the trough. The intrusion transports the offshore warm water shoreward into the fjord to alter water properties (Håvik & Våge, 2018) in a way that is not diminished during the subsequent return of the winds to downwelling-favorable (Figure 2f-h). For this reason, even if the intruding AW is not advected into the fjord immediately, each upwelling event can bring some amount of AW onto the shelf nearer to shore that can be delivered into the fjord and enhance warming there during subsequent events (Kämpf, 2006; Fraser et al., 2018). During weak wind events, the oscillatory shelf flows are weak with a low Rossby number (Kämpf, 2009; Lentz et al., 2014), and would not produce net onshore intrusion of the offshore warm AW. This explains why only some wind-driven intermediary circulation within Sermilik Fjord results in advection of warm waters into the fjord (Jackson et al., 2014, 2018).

Our observations in Sermilik Trough of the appearance of warm water at the surface (upwelling and inflow), at depth (warming from inflow at depth), and the timing of the appearance (<1 day lag with upwelling-favorable winds) is consistent with bathymetrically-induced localized onshore intrusion flow of warm AW. A back-of-the-envelope estimate based on the observed warm water surface signals in MODIS indicates that the intrusion velocities in the cross-shelf (along-trough) direction is at least 0.13-0.19 m/s. While we find good agreement with previous studies (She & Klinck, 2000; Kämpf, 2007; Lentz et al., 2014; Zhang & Lentz, 2017), those environments (e.g., Hudson Shelf Valley) differ from the Sermilik system where the EGCC may slow down at times, but not always reverse, during upwelling-favorable winds (Sutherland & Pickart, 2008), which likely suppresses the coastal-trapped waves. Future work to model the Sermilik system (i.e., a nonlinear trough carved into an undulating continental shelf that leads to a fjord where there is a background current and strong stratification) would be needed to confirm our findings.

AW inflow into the fjord likely results from the concurrent wind-driven intermediary circulation within the fjord. During the intrusions, we observe intermediary circulation as outflow at the surface, which results from the relaxation of downwelling-favorable winds and/or the onset of upwelling-favorable winds. This outflow indicates the draining of PW out of the fjord at the surface, which corresponds with a compensating AW inflow of at depth (Stigebrandt, 1981; Klinck et al., 1981; Straneo et al., 2010). Intermediary circulation explains the advection of warm water - that leads to subsurface warming at multiple depths within the fjord ($\Delta T_{4:8,-4:8}$ is 0.30±0.19°C at 250 m, 0.17±0.09°C at 350 m, and 0.09±0.07°C at 400 m) - into Sermilik Fjord toward Helheim Glacier during AW intrusions.

While wind-driven intrusions advect AW inshore, the EGCC likely serves as a barrier to AW intrusions, both by increasing the physical distance that AW must travel to reach Sermilik Fjord, and by enhancing ambient shelf stratification that suppresses inshore intrusion flow in the surface layer. Narrowing of the EGCC allows a more efficient intrusion of AW onto the shelf by reducing the distance AW must travel to reach the fjord and the extent to which the water dilutes along the way (Snow et al., 2021). Consistent with enhanced temperature variability observed at the subsurface shelf mooring (r^2=0.40; Figure S3), a wider EGCC seasonally also coincides with greater transport and increased stratification of the deeper water layers along the inner shelf (see Supplementary Information). Modeling suggests that strong stratification creates a lid over upwelling within the canyon and that isopycnals tend to squeeze together above the canyon below the surface layer (Ramos-Musalem & Allen, 2019). A deeper pycnocline suppresses the vertical extent of the bathymetrical influence and, thus, reduces the chance of upwelling flow reaching the surface. This vertical suppression of the intrusions would limit our ability to observe them, and restrict the depth range that AW is transported toward the head of the trough. Greater sea ice concentrations within the EGCC also decouples wind and surface ocean stresses over the trough, which we speculate would reduce or completely diminish the intensity of the inflow, though this has not been tested. While greater influence by the EGCC likely suppresses intrusions, we note that a lack of surface expression does not preclude the intrusions from still occurring at depth (Figure 1c).

We further speculate that greater wind forcing is required to produce intrusions and, thus, enhanced inshore heat transport when the EGCC widens and deepens. Simple-model results suggest that intrusions resulting from upwelling-favorable winds intensify throughout the first 24 hours and remain at these elevated velocities as long as the winds persisted (Zhang & Lentz, 2017). Based on water velocities during the intrusions and the time over which they develop, this would suggest that the strength and duration of an upwelling alongshore wind configuration could greatly affect overall transport of AW during an event. Stratification also diffuses over time by vertical turbulence as upwelling continues (Ramos-Musalem & Allen, 2019), making it more likely for the intrusion to extend upwards in the water column with time. Differences in wind event duration and magnitude or EGCC width during an intrusion likely regulate when the wind events effectively transport AW into the fjord. Offshore AW temperature variability and the depth of inflow also likely moderates whether warming or cooling is observed inshore and within the fjord (Fraser et al., 2018).

Herein we show that many wind-driven intrusions result in warm offshore water being pumped onto the continental shelf and sometimes into Sermilik Fjord. If more frequent upwelling-favorable wind events and less freshwater transport within the EGCC were to occur, this would be expected to lead to higher volumes of AW, and heat, flushing onto the shelf and into Sermilik Fjord. Greater cyclone activity, specific high pressure blocking patterns, and a high NAO index, which relates to storm variability in southeastern Greenland (Harden et al., 2011; Straneo & Heimbach, 2013), could all make intrusions more common. Further, weakening of the EGCC as a result of reduced freshwater and sea ice transport out of the Arctic (Harden et al., 2014), enhanced ejection of PW off the continental shelf, and runoff/iceberg calving from the Greenland Ice Sheet (Sutherland & Pickart, 2008) will reduce the dilution of AW as it crosses the continental shelf and make southeast Greenland fjords more susceptible to warm water inflow (Murray et al., 2010; Snow et al., 2021). Models may be able to predict anomalously high heat transport years using this improved understanding of the linkage between subsurface water temperatures, EGCC width/transport, and intrusion-favorable wind events. As has been demonstrated herein, a better understanding of deep-water heat transport changes that may directly feed into Sermilik Fjord and bring heat to Helheim Glacier both projected into the past and future has substantial implications for pinpointing the role of the ocean in glacier change. Intrusions of this nature may also occur to varying extents at other glacier systems around Greenland, such as Kangerdlugssuaq Glacier (Fraser et al., 2018), which could make it an important mechanism for regulating large-scale ice sheet dynamical mass loss.

Acknowledgments

We gratefully acknowledge the National Aeronautics and Space Administration (NASA), the U.S. National Science Foundation (NSF), and the Cooperative Institute for Research in Environmental Sciences (CIRES). This work was supported by NASA Headquarters under a NASA Earth and Space Science Fellowship Program – Grant (NNX16AO33H). This material is also based upon work supported by the NSF Graduate Research Fellowship Program under grant DGE1650115. Any opinions, findings, and conclusions or recommendations expressed in this material are those of the authors and do not necessarily reflect the views of the NSF. We thank Kathleen Bogan (CIRES) for her artistic design of Figure 1b,c. Processed data used in this manuscript is permanently archived at the Arctic Data Center (doi:—–). The Python Jupyter Notebook processing and analysis code is available at `---`. Users of the code should contact the author to ensure reasonable applications of the method. The Sermilik Fjord mouth mooring data used in this paper is available at the National Oceanographic Data Center (`https://data.nodc.noaa.gov/cgi-bin/iso?id=gov.noaa.nodc:0127325` and 0127320). Sea surface height data was provided by B. Harden. Level 2 MODIS visible and thermal infrared imagery can be found at search.earthdata.nasa.gov, and ECMWF ERA-5 data is located at www.ecmwf.int. Thanks also go to the two reviewers for their comments that greatly improved the quality of this paper.

References

Allen, S. E., & Hickey, B. M. (2010). Dynamics of advection-driven upwelling over a shelf break submarine canyon. *Journal of Geophysical Research: Oceans (1978–2012)*, *115*(C8). doi: 10.1029/2009jc005731

Allen, S. E., & Madron, X. D. d. (2009). A review of the role of submarine canyons in deep-ocean exchange with the shelf. *Ocean Science*, *5*(4), 607–620. doi: 10.5194/os-5-607-2009

Andresen, C. S., Straneo, F., Ribergaard, M. H., Bjørk, A. A., Andersen, T. J., Kuijpers, A., … Ahlstrøm, A. P. (2012). Rapid response of Helheim Glacier in Greenland to climate variability over the past century. *Nature Geoscience*, *5*(1), 37–41. doi: 10.1038/ngeo1349

Brearley, J. A., Pickart, R. S., Valdimarsson, H., Jonsson, S., Schmitt, R. W., & Haine, T. W. N. (2012). The East Greenland boundary current system south of Denmark Strait. *Deep Sea Research Part I: Oceanographic Research Papers*, *63*, 1–19. doi: 10.1016/j.dsr.2012.01.001

Bruce, J. G. (1995). Eddies southwest of the Denmark Strait. *Deep Sea Research Part I: Oceanographic Research Papers*, *42*(1), 13–29. doi: 10.1016/0967-0637(94)00040-y

Copernicus Climate Change Service. (2017). *ERA5: Fifth generation of ECMWF atmospheric reanalyses of the global climate.* https://cds.climate.copernicus.eu. (Accessed: 2018-11-04)

Cowton, T., Sole, A., Nienow, P., Slater, D., & Hanna, E. (2016). Controls on the transport of oceanic heat to Kangerdlugssuaq Glacier, East Greenland. *Journal of Glaciology*, *62*(236), 1167–1180. doi: 10.1017/jog.2016.117

Crawford, A. D., Alley, K. E., Cooke, A. M., & Serreze, M. C. (2020). Synoptic Climatology of Rain-on-Snow Events in Alaska Synoptic Climatology of Rain-on-Snow Events in Alaska. *Monthly Weather Review*, *148*(3), 1275–1295. doi: 10.1175/mwr-d-19-0311.1

Crawford, A. D., & Serreze, M. C. (2016). Does the Summer Arctic Frontal Zone Influence Arctic Ocean Cyclone Activity? *Journal of Climate*, *29*(13), 4977–4993. doi: 10.1175/jcli-d-15-0755.1

Enderlin, E. M., Howat, I. M., Jeong, S., Noh, M., Angelen, J. H., & van den Broeke, M. R. (2014). An improved mass budget for the Greenland ice sheet. *Geophysical Research Letters*, *41*(3), 866–872. doi: 10.1002/2013GL059010

Fraser, N. J., Inall, M. E., Magaldi, M. G., Haine, T. W. N., & Jones, S. C. (2018). Wintertime Fjord-Shelf Interaction and Ice Sheet Melting in Southeast Greenland. *Journal of Geophysical Research: Oceans*, *123*(12), 9156–9177. doi: 10.1029/2018jc014435

Hampson, P. (2020). *Glacial Troughs Eject Wind-Driven Shelf Circulation to the Slope* (Unpublished doctoral dissertation).

Harden, B., Renfrew, I., & Petersen, G. (2011). A Climatology of Wintertime Barrier Winds off Southeast Greenland. *Journal of Climate*, *24*(17), 4701–4717. doi: 10.1175/2011JCLI4113.1

Harden, B., Straneo, F., & Sutherland, D. (2014). Moored observations of synoptic and seasonal variability in the East Greenland Coastal Current. *Journal of Geophysical Research: Oceans*, *119*(12), 8838–8857. doi: 10.1002/2014JC010134

Holland, D. M., Thomas, R. H., Young, B. d., Ribergaard, M. H., & Lyberth, B. (2008). Acceleration of Jakobshavn Isbræ triggered by warm subsurface ocean waters. *Nature Geoscience*, *1*, 659. doi: 10.1038/ngeo316

Howat, I. M., Joughin, I., Fahnestock, M., Smith, B., & Scambos, T. (2008). Synchronous retreat and acceleration of southeast Greenland outlet glaciers 2000–06: Ice dynamics and coupling to climate. *Journal of Glaciology*, *54*(187).

Håvik, L., & Våge, K. (2018). Wind-Driven Coastal Upwelling and Downwelling in the Shelfbreak East Greenland Current. *Journal of Geophysical Research: Oceans*, *123*(9), 6106–6115. doi: 10.1029/2018jc014273

IMBIE Team, T. (2019). Mass balance of the Greenland Ice Sheet from 1992 to 2018. *Nature*. doi: 10.1038/s41586-019-1855-2

Jackson, R. H., Lentz, S. J., & Straneo, F. (2018). The Dynamics of Shelf Forcing in Greenlandic Fjords. *Journal of Physical Oceanography*, *48*(11), 2799–2827. doi: 10.1175/jpo-d-18-0057.1

Jackson, R. H., & Straneo, F. (2016). Heat, Salt, and Freshwater Budgets for a Glacial Fjord in Greenland. *Journal of Physical Oceanography*, *46*(9), 2735–2768. doi: 10.1175/JPO-D-15-0134.1

Jackson, R. H., Straneo, F., & Sutherland, D. A. (2014). Externally forced fluctuations in ocean temperature at Greenland glaciers in non-summer months. *Nature Geoscience*, *7*(7), 503–508. doi: 10.1038/ngeo2186

Johannessen, O. M., Korablev, A., Miles, V., Miles, M. W., & Solberg, K. E. (2011). Interaction Between the Warm Subsurface Atlantic Water in the Sermilik Fjord and Helheim Glacier in Southeast Greenland. *Surveys in Geophysics*, *32*(4-5), 387. doi: 10.1007/s10712-011-9130-6

Klinck, J. M., O'Brien, J. J., & Svendsen, H. (1981). A Simple Model of Fjord and

Coastal Circulation Interaction. *Journal of Physical Oceanography*, *11*(12), 1612–1626.

Kämpf, J. (2006). Transient wind-driven upwelling in a submarine canyon: A process-oriented modeling study. *Journal of Geophysical Research: Oceans (1978–2012)*, *111*(C11). doi: 10.1029/2006jc003497

Kämpf, J. (2007). On the magnitude of upwelling fluxes in shelf-break canyons. *Continental Shelf Research*, *27*(17), 2211–2223. doi: 10.1016/j.csr.2007.05.010

Kämpf, J. (2009). On the Interaction of Time-Variable Flows with a Shelfbreak Canyon. *Journal of Physical Oceanography*, *39*(1), 248–260. doi: 10.1175/2008jpo3753.1

Le Bras, I., Straneo, F., Holte, J., & Holliday, P. N. (2018). Seasonality of Freshwater in the East Greenland Current System From 2014 to 2016. *Journal of Geophysical Research: Oceans*. doi: 10.1029/2018JC014511

Lentz, S. J., Butman, B., & Harris, C. (2014). The vertical structure of the circulation and dynamics in Hudson Shelf Valley. *Journal of Geophysical Research: Oceans*, *119*(6). doi: 10.1002/2014jc009883

Magaldi, M. G., Haine, T. W. N., & Pickart, R. S. (2011). On the Nature and Variability of the East Greenland Spill Jet: A Case Study in Summer 2003*. *Journal of Physical Oceanography*, *41*(12), 2307–2327. doi: 10.1175/jpo-d-10-05004.1

Millan, R., Rignot, E., Mouginot, J., Wood, M., Bjørk, A., & Morlighem, M. (2018). Vulnerability of Southeast Greenland Glaciers to Warm Atlantic Water From Operation IceBridge and Ocean Melting Greenland Data. *Geophysical Research Letters*, *45*(6), 2688–2696. doi: 10.1002/2017GL076561

Morlighem, M., Williams, C. N., Rignot, E., An, L., Arndt, J. E., Bamber, J. L., … Zinglersen, K. B. (2017). BedMachine v3: Complete Bed Topography and Ocean Bathymetry Mapping of Greenland From Multibeam Echo Sounding Combined With Mass Conservation. *Geophysical research letters*, *44*(21), 11051–11061. doi: 10.1002/2017gl074954

Mouginot, J., Rignot, E., Bjørk, A. A., van den Broeke, M., Millan, R., Morlighem, M., … Wood, M. (2019). Forty-six years of Greenland Ice Sheet mass balance from 1972 to 2018. *Proceedings of the National Academy of Sciences*, *116*(19), 9239–9244. doi: 10.1073/pnas.1904242116

Mouginot, J., Rignot, E., Scheuchl, B., Fenty, I., Khazendar, A., Morlighem, M., ... Paden, J. (2015). Fast retreat of Zachariæ Isstrøm, northeast Greenland. *Science*, *350*(6266), 1357–1361. doi: 10.1126/science.aac7111

Murray, T., Scharrer, K., James, T., Dye, S., Hanna, E., Booth, A., ... Huybrechts, P. (2010). Ocean regulation hypothesis for glacier dynamics in southeast Greenland and implications for ice sheet mass changes. *Journal of Geophysical Research: Earth Surface (2003–2012)*, *115*(F3). doi: 10.1029/2009JF001522

Oltmanns, M., Straneo, F., Moore, G., & Mernild, S. (2014). Strong Downslope Wind Events in Ammassalik, Southeast Greenland. *Journal of Climate*, *27*(3), 977–993. doi: 10.1175/JCLI-D-13-00067.1

Ramos-Musalem, K., & Allen, S. E. (2019). The impact of locally-enhanced vertical diffusivity on the cross-shelf transport of tracers induced by a submarine canyon The impact of locally-enhanced vertical diffusivity on the cross-shelf transport of tracers induced by a submarine canyon. *Journal of Physical Oceanography*, *49*(2), 561–584. doi: 10.1175/jpo-d-18-0174.1

Rudels, B., Fahrbach, E., Meincke, J., Budéus, G., & Eriksson, P. (2002). The East Greenland Current and its contribution to the Denmark Strait overflow. *ICES Journal of Marine Science*, *59*(6), 1133–1154. doi: 10.1006/jmsc.2002.1284

Sciascia, R., Cenedese, C., Nicolì, D., Heimbach, P., & Straneo, F. (2014). Impact of periodic intermediary flows on submarine melting of a Greenland glacier. *Journal of Geophysical Research: Oceans*, *119*(10), 7078–7098. doi: 10.1002/2014jc009953

She, J., & Klinck, J. M. (2000). Flow near submarine canyons driven by constant winds. *Journal of Geophysical Research: Oceans*, *105*(C12), 28671–28694. doi: 10.1029/2000jc900126

Smith, B., Fricker, H. A., Gardner, A. S., Medley, B., Nilsson, J., Paolo, F. S., ... Zwally, H. J. (2020). Pervasive ice sheet mass loss reflects competing ocean and atmosphere processes. *Science*, *368*(6496), 1239–1242. doi: 10.1126/science.aaz5845

Snow, T., Straneo, F., Holte, J., Grigsby, S., Abdalati, W., & Scambos, T. (2021). More than skin deep: sea surface temperature as a means of inferring Atlantic Water variability on the southeast Greenland continental shelf near Helheim Glacier. *Journal of Geophysical Research: Oceans*. doi:

https://www.essoar.org/doi/abs/10.1002/essoar.10503490.1

Stigebrandt, A. (1981). A mechanism governing the estuarine circulation in deep, strongly stratified fjords. *Estuarine, Coastal and Shelf Science*, *13*(2), 197–211. doi: 10.1016/s0302-3524(81)80076-x

Straneo, F., Curry, R., Sutherland, D., & Hamilton, G. (2011). Impact of fjord dynamics and glacial runoff on the circulation near Helheim Glacier. *Nature Geoscience*, *4*. doi: 10.1038/ngeo1109

Straneo, F., Hamilton, G. S., Sutherland, D. A., Stearns, L. A., Davidson, F., Hammill, M. O., ... Rosing-Asvid, A. (2010). Rapid circulation of warm subtropical waters in a major glacial fjord in East Greenland. *Nature Geoscience*, *3*(3), 182. doi: 10.1038/ngeo764

Straneo, F., & Heimbach, P. (2013). North Atlantic warming and the retreat of Greenland's outlet glaciers. *Nature*, *504*(7478), 36–43. doi: 10.1038/nature12854

Sutherland, D. A., & Pickart, R. S. (2008). The East Greenland Coastal Current: Structure, variability, and forcing. *Progress in Oceanography*, *78*(1), 58–77. doi: 10.1016/j.pocean.2007.09.006

Sutherland, D. A., Straneo, F., & Pickart, R. S. (2014). Characteristics and dynamics of two major Greenland glacial fjords. *Journal of Geophysical Research: Oceans*, *119*(6), 3767–3791. doi: 10.1002/2013JC009786

Sutherland, D. A., Straneo, F., Stenson, G. B., Davidson, F., Hammill, M. O., & Rosing-Asvid, A. (2013). Atlantic water variability on the SE Greenland continental shelf and its relationship to SST and bathymetry. *Journal of Geophysical Research: Oceans*, *118*(2), 847–855. doi: 10.1029/2012JC008354

Svendsen, H., & Thompson, R. O. R. Y. (1978). Wind-Driven Circulation in a Fjord. *Journal of Physical Oceanography*, *8*(4), 703–712.

Våge, K., Pickart, R. S., Sarafanov, A., Knutsen, O., Mercier, H., Lherminier, P., ... Bacon, S. (2011). The Irminger Gyre: Circulation, convection, and interannual variability. *Deep Sea Research Part I: Oceanographic Research Papers*, *58*(5), 590–614. doi: 10.1016/j.dsr.2011.03.001

Zhang, W. G., & Lentz, S. J. (2017). Wind-Driven Circulation in a Shelf Valley. Part I: Mechanism of the Asymmetrical Response to Along-Shelf Winds in Opposite Directions. *Journal of Physical Oceanography*, *47*(12), 2927–2947.

doi: 10.1175/jpo-d-17-0083.1

Supporting Information for "Alongshore winds force warm Atlantic Water toward Helheim Glacier in southeast Greenland"

T. Snow[1,2,3], W. Zhang[4], E. Schreiber[5], W. Abdalati[2,3], T. Scambos[2]

[1]Colorado School of Mines, Department of Geophysics, Golden, CO, USA

[2]Cooperative Institute for Research in Environmental Sciences, University of Colorado, Boulder, CO, USA

[3]University of Colorado Boulder, Geography Department, Boulder, CO, USA

[4]Applied Ocean Physics and Engineering Department, Woods Hole Oceanographic Institution, Woods Hole, MA, USA

[5]UNAVCO, 6350 Nautilus Drive, Boulder, CO, 80301, USA

Contents of this file

Introduction The text and figures included in this supplement provide additional information and context supporting the conclusion of the main text.

Text S1. ERA-5 wind data analysis To determine the atmospheric variability associated with the Atlantic Water (AW) intrusions, we use the ERA-5 6-hourly 2-m wind field, instantaneous eastward and northward turbulent surface stresses, and mean sea level pressure fields on a 0.5°x 0.5°grid. From the ERA-5 U and V wind speeds and stress, we calculate alongshore winds as the velocity/stress component traveling along the principal axis of 242°from north at the shelf break. We produce a time series of wind direction and alongshore wind stress from 2010 to 2013 for comparison to the dates of the intrusions. At each time, the wind direction, speed, and stress are averaged across the mouth region of Sermilik Trough (between 64.4°-65.0°N, -38.0°–35.0°E; Figure 1a), where winds have the strongest correlation with changes in regional EGCC transport and the greatest impact on trough transport (Harden et al., 2014; Le Bras et al., 2018). Piteraq events (or Downslope Wind Events) are identified as >10 m/s winds between 270 and 20°(clockwise) averaged over the Tasiilaq region (65.5°-65.7°N, -37.82°E–37.42°E) following Oltmanns, Straneo, Moore, and Mernild (2014) (Figure 1a).

Text S2. Ocean mooring records The shelf and mid-fjord mooring instruments provide ocean temperature records during the AW intrusions. For the shelf mooring, we use the temperatures recorded by one instrument each year, either a Microcat SBE37SM or XR 420 RBR sensor, deployed between 262 and 301 m near the mouth of Sermilik Fjord. The mid-fjord mooring was deployed between 250-294, 324-350, 390-400, and 550-560 m depth (representing the 250, 350, 400, and 550 m records, respectively) and recorded temperatures using similar instruments as the shelf mooring (Jackson et al., 2014). Temperatures were acquired at 7.5-15 min intervals and averaged to 6-hourly.

Text S3. EGCC width and transport As a fresher water mass running along the coastline, the size of the EGCC may moderate the AW intrusions by serving as a barrier or diluting the intrusions as they cross the continental shelf (Snow et al., 2021). We use satellite-based calculations of the EGCC width in accordance with Snow et al. (2021) to indicate the size of the EGCC. We use the MODIS Level 3 SST V2014 products (Minnett et al., 2019). MODIS SSTs were sampled from the same shelf trough transect as Snow et al. (2021) (thirteen 14x14 km sampling boxes) and the SST anomaly relative to the Irminger Current temperature was then calculated and averaged to weekly. We approximated the EGCC width along the trough by measuring the distance from the fjord mouth (65.6°N,-38.0°E) to the center of the last sampling box along the trough transect that had a SST anomaly $<$-1.5°C (threshold delineating between PW at the surface within the EGCC and AW from the IC; Snow et al., 2021).

We observe enhanced temperature variability at the subsurface shelf mooring (r^2=0.40; Figure S3) when the EGCC is wider, which is consistent with greater transport within the EGCC. A wider EGCC seasonally coincides with greater transport and a deepening of the current (Harden et al., 2014), which stratifies deeper water layers along the inner shelf. Higher variability at the mooring sensor (290 m) indicates a deeper PW/AW interface that is normally located between 150-250 m depth (Harden et al., 2014; Jackson et al., 2014). Therefore, we use EGCC width as an indicator for EGCC transport.

Text S4. Atmosphere and ocean cross-correlation analyses To investigate the linkages between atmospheric and ocean records, we smoothed all records with a 30-hour second-order Butterworth filter and performed cross-correlation analyses between them. Across the four-year record, the shelf and fjord mooring temperatures lagged alongshore wind stress by ∼24 hours and 30 hours, respectively (Figure S4b). At these lags, ocean temperatures negatively correlated with alongshore wind stress (r=-0.19, -0.22, and -0.24, for the shelf at 290 m, mid-fjord at 250 m and mid-fjord at 350 m depth, respectively; $p<0.001$). SSH lagged alongshore wind stress by ∼6 hrs (Figure S4a) and ocean temperatures at each of the mooring sites had a stronger negative correlation with SSH (r=-0.33, -0.32, and -0.33, respectively; $p<0.001$) than with alongshore winds. The shelf warming followed a drop in SSH by 6 hours, while the mid-fjord warming followed the shelf SSH drop by 24 hrs (Figure S4c). These negative correlations are consistent with a downwelling-to-upwelling switch in coastal conditions and the observed lags are consistent with (Jackson et al., 2014).

References

Harden, B., Straneo, F., & Sutherland, D. (2014). Moored observations of synoptic and seasonal variability in the East Greenland Coastal Current. *Journal of Geophysical Research: Oceans*, *119*(12), 8838–8857. doi: 10.1002/2014JC010134

Jackson, R. H., Straneo, F., & Sutherland, D. A. (2014). Externally forced fluctuations in ocean temperature at Greenland glaciers in non-summer months. *Nature Geoscience*, *7*(7), 503–508. doi: 10.1038/ngeo2186

Le Bras, I., Straneo, F., Holte, J., & Holliday, P. N. (2018). Seasonality of Freshwater in the East Greenland Current System From 2014 to 2016. *Journal of Geophysical Research: Oceans*. doi: 10.1029/2018JC014511

Minnett, P., Alvera-Azcárate, A., Chin, T., Corlett, G., Gentemann, C., Karagali, I., . . . Vazquez-Cuervo, J. (2019). Half a century of satellite remote sensing of sea-surface temperature. *Remote Sensing of Environment*, *233*, 111366. doi: 10.1016/

j.rse.2019.111366

Oltmanns, M., Straneo, F., Moore, G., & Mernild, S. (2014). Strong Downslope Wind Events in Ammassalik, Southeast Greenland. *Journal of Climate*, *27*(3), 977–993. doi: 10.1175/JCLI-D-13-00067.1

Snow, T., Straneo, F., Holte, J., Grigsby, S., Abdalati, W., & Scambos, T. (2021). More than skin deep: sea surface temperature as a means of inferring Atlantic Water variability on the southeast Greenland continental shelf near Helheim Glacier. *Journal of Geophysical Research: Oceans*. doi: https://www.essoar.org/doi/abs/10.1002/essoar.10503490.1

Table S1: AW intrusions identified from MODIS visible imagery and ERA-5 alongshore wind stress.

Beginning of Table S1			
Date Time	Image Date	Piteraq [T/F]	EGCC width [km]
2010-01-23 18:00:00	2010-01-24	1	75.5
2010-02-16 06:00:00	2010-02-17	0	75.5
2010-03-05 06:00:00	2010-03-05	1	75.5
2010-03-11 18:00:00	2010-03-12	0	90.1
2010-03-14 18:00:00	2010-03-15	0	90.1
2010-03-25 18:00:00	2010-03-26	0	60.6
2010-03-30 06:00:00	2010-03-31	0	60.6
2010-04-06 12:00:00	2010-04-06	0	90.1
2010-04-11 12:00:00	2010-04-11	0	90.1
2010-04-16 18:00:00	2010-04-16	0	90.1
2010-04-30 12:00:00	2010-04-30	0	75.5
2010-05-05 18:00:00	2010-05-06	0	75.5
2011-01-24 18:00:00	2011-01-24	0	75.5
2011-02-15 12:00:00	2011-02-17	0	46.0
2011-02-25 18:00:00	2011-02-26	1	60.6
2011-03-03 00:00:00	2011-03-03	0	90.1
2011-03-06 06:00:00	2011-03-06	1	90.1
2011-03-25 18:00:00	2011-03-26	0	110.3
2011-04-11 00:00:00	2011-04-11	0	110.3
2011-04-14 06:00:00	2011-04-14	0	110.3
2011-04-19 06:00:00	2011-04-19	1	110.3
2011-05-08 18:00:00	2011-05-09	0	75.5
2011-05-23 12:00:00	2011-05-23	0	75.5
2011-06-01 18:00:00	2011-06-01	0	90.1
2012-01-25 18:00:00	2012-01-26	0	75.5
2012-01-29 12:00:00	2012-01-29	0	75.5
2012-02-09 18:00:00	2012-02-10	0	31.4
2012-02-15 00:00:00	2012-02-16	0	90.1
2012-03-09 06:00:00	2012-03-09	0	130.5
2012-03-14 00:00:00	2012-03-14	0	110.3
2012-03-27 06:00:00	2012-03-27	0	110.3
2012-04-03 00:00:00	2012-04-03	0	90.1
2012-04-05 18:00:00	2012-04-06	0	90.1
2012-04-13 00:00:00	2012-04-13	0	150.7
2012-04-20 06:00:00	2012-04-20	0	60.6
2012-04-27 06:00:00	2012-04-28	0	60.6
2012-04-30 12:00:00	2012-05-01	0	60.6
2012-05-02 18:00:00	2012-05-03	0	60.6

Continuation of Table S1			
Date Time	Image Date	Piteraq [T/F]	EGCC width [km]
2012-05-25 12:00:00	2012-05-26	0	110.3
2012-06-11 06:00:00	2012-06-11	0	-
2012-06-15 00:00:00	2012-06-16	0	-
2012-06-18 00:00:00	2012-06-19	0	110.3
2012-06-25 00:00:00	2012-06-25	0	-
2013-01-28 18:00:00	2013-01-28	0	46.0
2013-02-04 12:00:00	2013-02-04	0	75.5
2013-03-01 06:00:00	2013-03-01	1	90.1
2013-03-12 00:00:00	2013-03-12	0	60.6
2013-03-21 18:00:00	2013-03-22	0	90.1
2013-04-08 18:00:00	2013-04-08	0	75.5
2013-04-23 00:00:00	2013-04-24	0	75.5
2013-05-08 00:00:00	2013-05-08	0	90.1
2013-05-20 12:00:00	2013-05-20	0	60.6
2013-06-16 00:00:00	2013-06-16	0	110.3

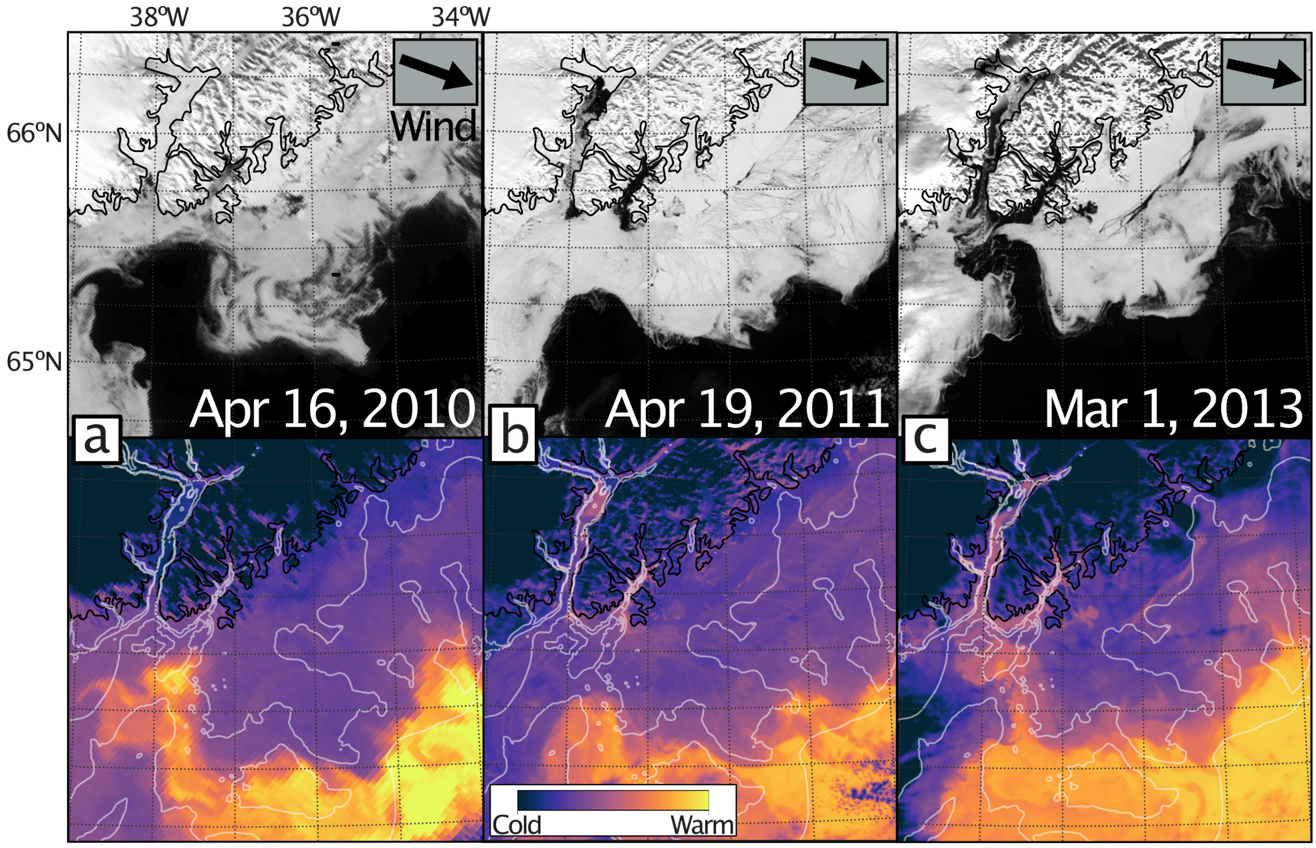

Figure S1. Three intrusions observed in MODIS imagery in the visible spectrum (top) and Band 31 (thermal infrared)-derived brightness temperatures (bottom) shown for (a) April 16, 2010, (b) April 19, 2011, and (c) March 1, 2013. Black arrows indicate wind direction.

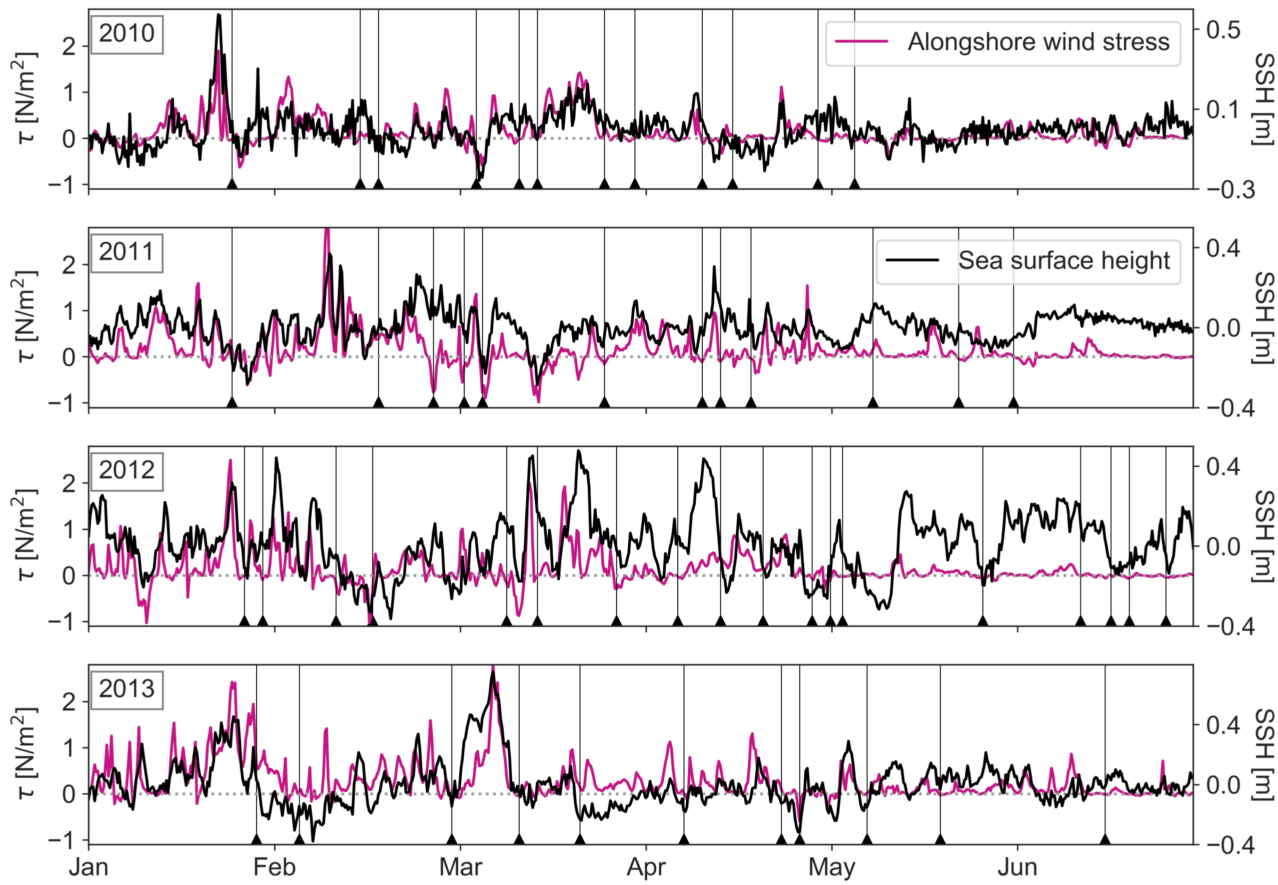

Figure S2. The dates of all MODIS-observed intrusions used in this study (vertical lines) in comparison to alongshore wind stress (purple lines; positive means northeasterly) and continental shelf sea surface height (SSH; black lines) records. The records span from January through June for each year.

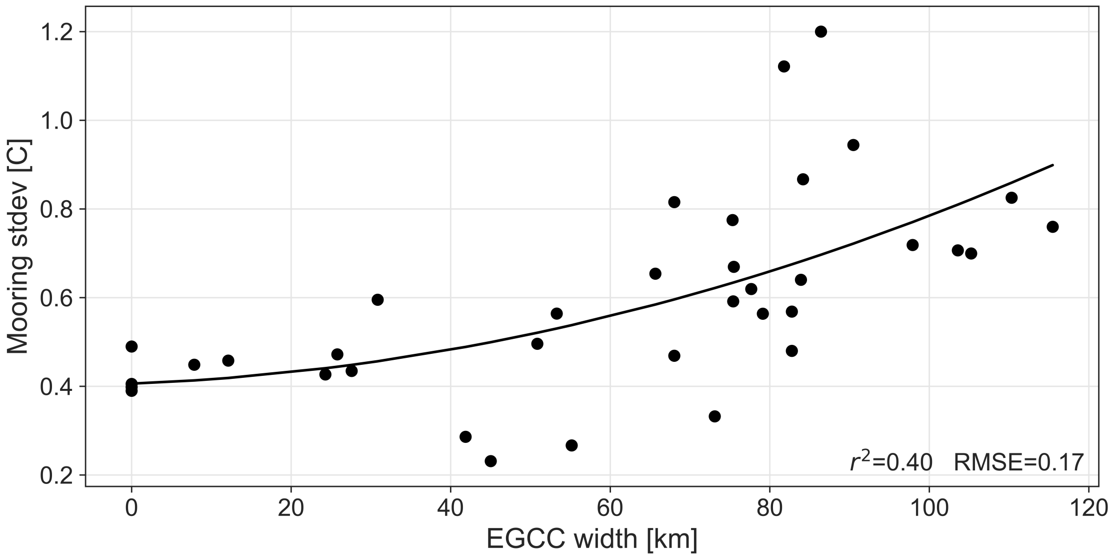

Figure S3. Standard deviation of monthly-aggregated moored subsurface ocean temperatures in comparison to sea surface temperature-derived EGCC width (circles). The second-order polynomial for the data (line), r^2, and root mean square error (RMSE) are shown.

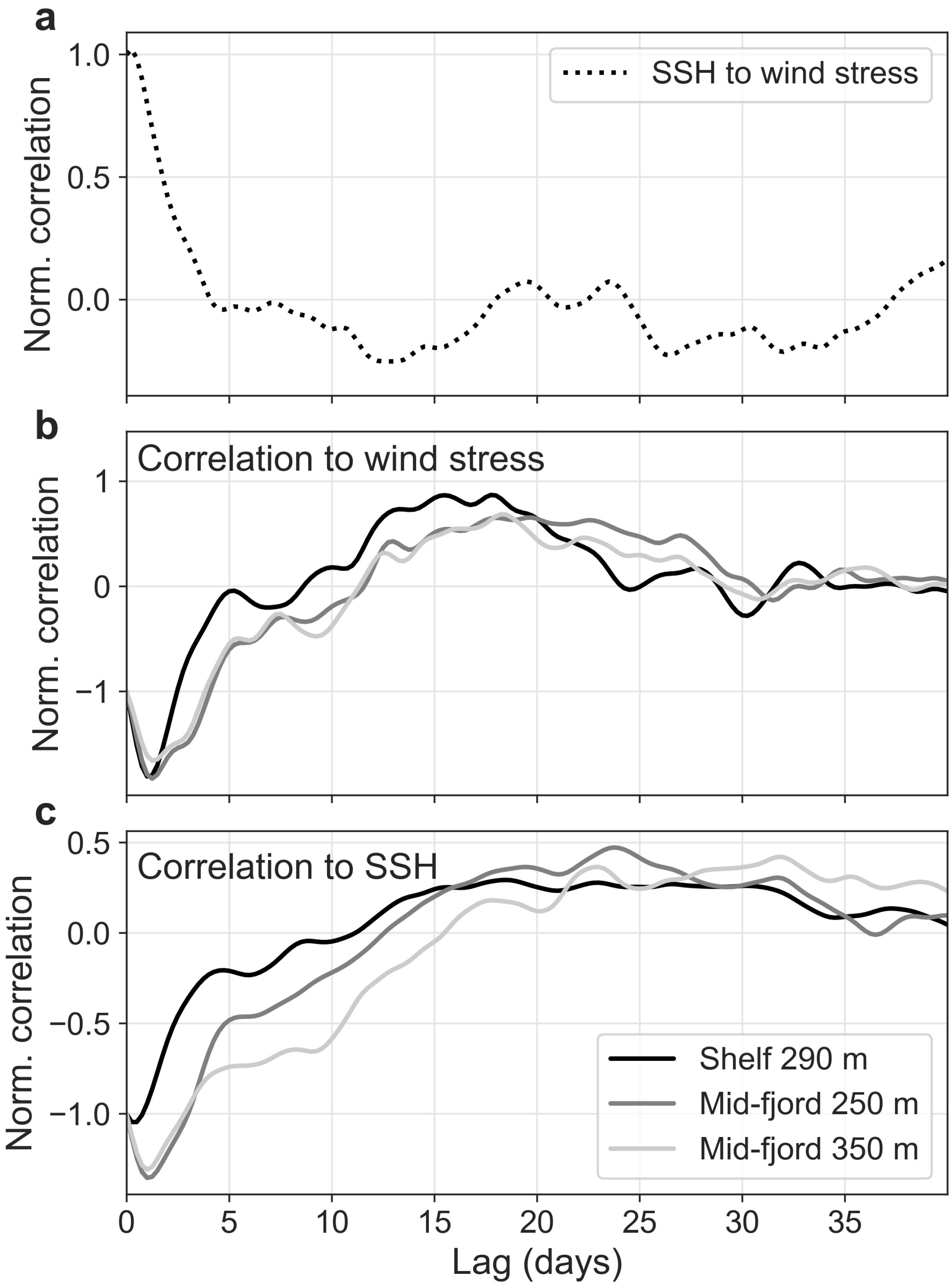

Figure S4. Cross-correlations between alongshore wind stress, sea surface height (SSH), and mooring temperature records. (a) Cross correlation of SSH and alongshore winds. Cross correlation of the shelf 290 m (black), mid-fjord 250 m (dark gray), and mid-fjord 350 m (light gray) mooring temperature records with (b) the alongshore wind stress and (c) SSH. All records were smoothed with a 30-hour second-order Butterworth filter.